arXiv:1807.11204v1 [astro-ph.GA] 30 Jul 2018

VEGAS: A VST Early-type GAlaxy Survey.
III. Mapping the galaxy structure, interactions and intragroup light in the NGC 5018 group

Marilena Spavone[1]

Enrichetta Iodice[1]

Massimo Capaccioli[2]

Daniela Bettoni[3]

Roberto Rampazzo[3]

Noah Brosch[4]

Michele Cantiello[5]

Nicola R. Napolitano[1]

Luca Limatola[1]

Aniello Grado[1]

Pietro Schipani[1]

[1] INAF-Astronomical Observatory of Capodimonte
Salita Moiariello 16, 80131, Naples, Italy
[2] University of Naples Federico II, C.U. Monte Sant'Angelo
via Cinthia, 80126, Naples, Italy
[3] INAF-Astronomical Observatory of Padova
Vicolo dell'Osservatorio 5, I-35122, Padova, Italy
[4] The Wise Observatory and School of Physics and Astronomy
Tel Aviv University, Israel
[5] INAF-Astronomical Observatory of Teramo
Via Maggini, 64100, Teramo, Italy

ABSTRACT

Most of the galaxies in the Universe at present day are in groups, which are key to understanding the galaxy evolution. In this work we present a new deep mosaic of 1.2×1.0 square degrees of the group of galaxies centered on NGC 5018, acquired at the ESO VLT Survey Telescope. We use u, g, r images to analyse the structure of the group members and to estimate the intra-group light. Taking advantage of the deep and multiband photometry and of the large field of view of the VST telescope, we studied the structure of the galaxy members and the faint features into the intra-group space and we give an estimate of the intragroup diffuse light in the NGC 5018 group of galaxies. We found that $\sim 41\%$ of the total g-band luminosity of the group is in the form of intragroup light (IGL). The IGL has a $(g$ - $r)$ color consistent with those of other galaxies in the group, indicating that the stripping

Corresponding author: Marilena Spavone
marilena.spavone@oacn.inaf.it

leading to the formation of IGL is ongoing. From the study of this group we can infer that there are at least two different interactions involving the group members: one between NGC 5018 and NGC 5022, which generates the tails and ring-like structures detected in the light, and another between NGC 5022 and MCG-03-34-013 that have produced the HI tail. A minor merging event also happened in the formation history of NGC 5018 that have perturbed the inner structure of this galaxy.

Keywords: surveys – galaxies: elliptical and lenticular, cD – galaxies: fundamental parameters – galaxies: formation – galaxies: halos – galaxies: groups: individual (NGC 5018)

1. INTRODUCTION

The hierarchical, merger-dominated picture of galaxy formation predicts that the observed galaxies and their dark halo (DH) were formed through repeated merging processes of small systems (De Lucia et al. 2006). Under this paradigm, clusters of galaxies are the most recent objects to form and their central galaxies continue to undergo active mass assembly and accretion of smaller groups.

Throughout this cluster assembly, individual galaxies interact with one other. During these interactions, matter can be stripped from galaxies and form tidal tails, shells, bridges, and liberating stars from their host galaxies, which contribute to formation of a very faint component of diffuse intacluster light (ICL) (Mihos 2015).

According to this picture, any star that becomes unbound from its host galaxy contributes to the growth of ICL, which can then be considered as the fossil record of all the past interactions. If so, the main properties of the ICL, such as color, metallicity, spatial distribution, are closely linked to the properties of galaxies in which intracluster stars are originated, and then can help to disentangle their formation history.

In the group environment, interactions between galaxies are slow leading to a strong tidal stripping of material and to the formation of tidal debris, which are mixed into the ICL when the groups fall into the cluster. In situ star formation can also occur in the intracluster medium, due to the presence of gas stripped from infalling galaxies, contributing to feed the ICL. Following this evolutionary picture, the diffuse intragroup light (IGL) can be considered as a precursor to the ICL in massive clusters of galaxies.

Since groups contain most of the galaxies in the Universe ($\sim 60\%$) at present day, the group environment is of particular interest for the study of the intragroup starlight. IGL is in fact quite evident in strongly interacting groups, given that the strong interactions are able to expel diffuse material out to large distances (Da Rocha & Mendes de Oliveira 2005; Watkins et al. 2015).

In the last decade, a big effort was made to determine the amount and spatial distribution of intragroup light in both normal and compact groups, both on the observational and on the theoretical side.

Theoretical studies give conflicting predictions on the fraction of the IGL component and of its variation with the group mass. Numerical simulations by Napolitano et al. (2003); Lin & Mohr (2004); Murante et al. (2004, 2007); Purcell et al. (2007); Watson et al. (2012); Tollet et al. (2017) predict a strong evolution of the ICL and IGL fraction with the cluster and group mass, while Krick & Bernstein (2007) found an anti-correlation between the ICL/IGL fraction and the cluster/group mass. Contini et al. (2014) found that the fractions of ICL and IGL predicted by their models range between 10% and 40% and that they don't vary as a function of the mass. Models by Sommer-Larsen (2006); Rudick et al. (2006) show that from 12% to 45% of the light in groups is in the form of IGL, and that the fractions of IGL/ICL can be used as a "dynamical clock", since they increase with the degree of dynamical evolution of the group/cluster (i.e. more evolved groups/clusters have largest fractions of diffuse light).

On the observational side, the diffuse IGL/ICL component has been mapped using several observational techniques, such as deep imaging (Feldmeier et al. 2002; Mihos et al. 2005; Zibetti et al. 2005), the detection of red giant branch stars associated with the diffuse stellar component (Williams et al. 2007), and intracluster planetary nebulae (Arnaboldi et al. 2002, 2004; Aguerri et al. 2005, 2006; Gerhard et al. 2005, 2007; Castro-Rodriguéz et al. 2009; Longobardi et al. 2013, 2015).

The fraction of IGL has been estimated in some compact groups of galaxies. Da Rocha & Mendes de Oliveira (2005); Da Rocha et al. (2008) found smooth envelopes of diffuse light around the studied galaxy groups, and estimated IGL fractions of 11%-46%, with colors compatible with those of galaxies in the groups. They also suggest an evolutionary sequence for the analyzed groups, i.e. groups with highest IGL fraction are in a more advanced phase of their dynamical evolution, with respect to groups with smaller fractions of IGL. Also White et al. (2003) found a consistent amount of IGL (38%-48%) in the compact group HCG 90, with a color distribution consistent with an old stellar population, while Aguerri

et al. (2006) found that an IGL fraction for the group HCG 44 of 4.7%. In contrast, Watkins et al. (2017) found no diffuse light in the M96 group. DeMaio et al. (2018) by studying the properties of 23 galaxy groups found that the Bright Cluster Galaxies (BCGs) together with the ICL constitute a higher fraction of the total mass in groups than in clusters, and that the group environments are more efficient ICL producers. McGee & Balogh (2010) by studying spectroscopically confirmed intragroup supernovae Ia, inferred that 47% of the stellar mass in the analyzed galaxy groups was in the form of IGL.

The study of intracluster planetary nebulae in two fields of the Virgo cluster, by Arnaboldi et al. (2004) , revealed that the diffuse light contributes from 17% to 43% of the total (i.e., galaxies + diffuse light) luminosity density in the imaged fields. Castro-Rodríguez et al. (2003), by carrying out a wide field survey for emission line objects associated with the intragroup HI cloud in the Leo group, have been able to set an upper limit for the ratio of diffuse intragroup to galaxy light that is $\sim$ 1.6%. Castro-Rodriguéz et al. (2009) by using planetary nebulae detected in several regions of the Virgo cluster, derived a fraction of ICL of $\sim$ 7% of the total light in Virgo cluster galaxies.

Recently, wide-field and deep photometric studies have revealed the presence of diffuse IGL even in the less dense environment of the loose groups (Ibata et al. 2014; Okamoto et al. 2015), where slow encounters are particularly effective at liberating stars from galaxies in the intragroup medium. Loose groups of galaxies are intermediate in scale between galaxies and rich clusters, and due to their irregular nature their definition is ambiguous. Their environment is also intermediate between that of isolated galaxies and that of the cores of rich clusters, and therefore the study of IGL in these environments is of particular interest, given that it can give clues on galaxy and galaxy cluster evolution.

Despite these many programs aimed at the study of the IGL/ICL in a variety of different systems in different dynamical states, there are still observational and interpretational difficulties to still face, which make the investigation of the IGL and ICL not a trivial task. Over the past decade many observational studies of these diffuse components have been carried out, but despite this the amount of ICL is hard to estimate. First, the fact that ICL and IGL components are diffuse and have very faint levels of surface brightness, which implies accurate techniques to correctly estimate all source of contamination, first the background. Second, the fact that the IGL/ICL is strictly connected to the BCGs and it is not always possible to distinguish from photometry only the diffuse (unbound) component from the extended (likely bound) stellar halos of the BCGs.

In the recent years, a great impulse to these researches has been given by deep photometric surveys aimed at studying galaxy structures out to the regions of the stellar halos, where the galaxy light merges into the intra-cluster component (Ferrarese et al. 2012; Duc et al. 2015; Muñoz et al. 2015; Merritt et al. 2016). The VST Early-type Galaxy Survey (VEGAS) (see http://www.na.astro.it/vegas/VEGAS/Welcome.html) is just a part of this campaign and it is producing competitive results. From the surface photometry for the cD galaxy NGC 4472, a tail of intracluster light was detected between $5R_e \leq R \leq 10R_e$, in the range of surface brightness of $26.5 - 27.6$ mag/arcsec^2 in the g band (Capaccioli et al. 2015). New results on six massive early-type galaxies (including NGC 4472) in the VEGAS, confirm the feasibility of such a survey to reach the faint surface brightness levels of $27 - 30$ mag/arcsec^2 in the g band, out to $\sim 10R_e$ (Spavone et al. 2017). Therefore, taking advantage of the deep photometry, the build up history of the stellar halo can be addressed by comparing the surface brightness profile and the stellar mass fraction with the prediction of cosmological galaxy formation.

As part of VEGAS, the *Fornax Deep Survey (FDS)* at VST covers the Fornax cluster out to the virial radius ($\sim$ 0.7 Mpc), with an area of about 26 square degrees around the central galaxy NGC 1399, and including the SW subgroup centered on Fornax A. First results have provided the up-to-date largest mosaics that covers an area of 3×6 square degrees around the central galaxy NGC 1399 (see the ESO photo release at https://www.eso.org/public/news/eso1612/) and an area of $\sim 4 \times 2$ square degrees around the central galaxy NGC 1316 of the SW group of the Fornax cluster (Iodice et al. 2016, 2017a). The deep photometry, the high spatial resolution of OmegaCam and the large covered area allow to map *i)* the surface brightness around NGC 1399 and NGC 1316 out to an unprecedented distance of $\sim$ 200 kpc down to $\mu_g \simeq 29 - 31$ mag/arcsec^2 (Iodice et al. 2016, 2017a); *ii)* to trace the spatial distribution of candidate Globular Clusters (GCs) inside ~ 0.5 deg^2 of the cluster core (D'Abrusco et al. 2016; Cantiello et al. 2018); *iii)* to detect new and faint ($\mu_g \simeq 28 - 30$ mag/arcsec^2) features in the intracluster region between NGC 1399 and NGC 1387 (Iodice et al. 2016) and in the outskirts of NGC 1316 (Iodice et al. 2017a); *iv)* to detect an unknown region of intra-cluster light (ICL) in the core of the cluster, on the West side of NGC 1399 (Iodice et al. 2017b).

Thanks to the coverage of different morphological types, masses and environments in VEGAS, we have started a study dedicated to the synoptic analysis of GC systems in different host galaxies. As an example, preliminary results from GCs in NGC3115 and NGC1399, support the scenario where the red/metal-rich GCs component is bound to the galaxy, while the blue/metal-poor GCs are gravitationally associated with a cluster-wide component, if present (Cantiello et al. 2018).

In this work we present a new deep mosaic of 1.2×1.0 square degrees of the group of galaxies centered on NGC 5018, acquired at the ESO VST. We use u, g, r images to analyse the structure of the group members and to estimate the intra-group light. This work represents a pilot study in the framework of the VEGAS survey to study the IGL components in the less dense environments of the groups.

We adopt a distance for NGC 5018 of D = 40.9 Mpc (Tully 1988), therefore the image scale is 198.3 parsecs/arcsec.

The plan of the paper is the following. In Sec. 2 we present the properties of NGC 5018 as found in the literature, while in Sec. 3 we describe the data used in this work, as well as the adopted observing strategy and the data reduction. In Sec. 4, 5 and 6 the photometric optical, infrared and UV analysis are described. In Sec. 7 we present the 1D fitting procedure adopted and the derived accreted mass fractions of galaxies in the group. In Sec. 8 we draw our conclusions.

2. NGC 5018 IN THE LITERATURE

NGC 5018 is the brightest member of a small group of five galaxies (Gourgoulhon et al. 1992), composed by the edge-on spiral, NGC 5022, the S0 galaxy MCG-03-34-013, and the two face-on dwarf, gas-rich ($\sim 10^8 M_\odot$) spirals labeled as S2 and S3 by Kim et al. 1988 (see Fig. 1). Kim et al. (1988), adopting a distance $D \sim 22.5h^{-1}$ Mpc, also estimate that the group has a size of ~ 200 kpc and a total mass of $\sim 4 \times 10^{12} M_\odot$. Despite its classification as "normal" elliptical, NGC 5018 shows several signs of a past interaction event, such as a very complex system of dust lanes, shells, a tail on the NW side, and a prominent bridge of gas toward the companion galaxy NGC 5022. The galaxy is also present in the list of shell galaxies revealed by Malin & Carter (1983).

The HI mass associated to NGC 5018, estimated by Kim et al. (1988), is $\sim 4 \times 10^8 M_\odot$, while the same authors found that the HI in NGC 5022 is distributed in a rotating disk, with a mass of $\sim 2 \times 10^9 M_\odot$.

Follow-up HI observations made by Guhathakurta et al. (1990), showed that the HI bridge actually connects NGC 5022 with MCG-03-34-013, while it bifurcates at

the position and radial velocity of NGC 5018. They also estimate that the interaction which led to the formation of the northern plume was recent ($\sim 6 \times 10^8$ Gyrs). Guhathakurta et al. (1990) assert that their HI and optical data provide the direct observational evidence for the formation of a shell system, through the merger of an elliptical galaxy with a cold disk system.

Many authors also found the presence of a young ($\sim$ 3 Gyrs) and dominant stellar population in the central regions of NGC 5018 (Bertola et al. 1993; Carollo & Danziger 1994; Leonardi & Worthey 2000; Buson et al. 2004; Rampazzo et al. 2007), with a near solar metallicity. The peculiarities found in NGC 5018, such as the lower metallicity with respect to the giant ellipticals, the presence of an Mg_2 index much weaker than those of ellipticals of similar absolute magnitude, the low UV flux level, the presence of bluer shells, a complex system of dust lanes, and a bridge of HI connecting NGC 5018 with NGC 5022, pose serious problems to the classical picture of elliptical galaxies formation.

Bertola et al. (1993) proposed two possible scenarios for the formation of this peculiar galaxy. The first scenario is the merging of many separate smaller galaxies, having low metallicities, while the other possibility is the formation ab initio with low metallicity and the subsequent, recent, merging with a small disk galaxy, which is able to reproduce the morphological peculiarities of NGC 5018. Bertola et al. (1993) discounted the dust obscuration as the cause of the low UV flux level because the best photometry available at that time showed that the dust lane does not cover the regions of their UV spectra. Later, Carollo & Danziger (1994) showed the presence of the dust till to the very central regions, demonstrating that the reddening effect was not negligible.

Leonardi & Worthey (2000) derived a robust reddening insensitive estimate of the age of the young stellar population in the central regions of NGC 5018. The estimated age of 2.8 Gyrs of this population, which dominates the visible part of the spectrum, also explain the small UV flux with no need to invoke a large amount of dust obscuration.

NGC 5018 has been examined by Rampazzo et al. (2013) using Spitzer-IRS spectrograph in Infrared, in the range 4-38 μm (see in particular their Figure 5). The galaxy nucleus shows Polycyclic Aromatic Hydrocarbon features (PAHs) with interband ratios typical of late-type galaxies. These PAH features are present only in 9^{+4}_{-3} fraction of early-type galaxies in the Revised Shapley-Ames catalogue examined by Rampazzo et al. (2013). This suggests that NGC 5018 has a still

actively star forming nuclear region, since IRS (SL+LL) spectra integrate in a projected region of 0.7×3.3 kpc.

Hilker & Kissler-Patig (1996) studied the properties of the globular clusters (GCs) of NGC 5018. They detect a poor globular cluster system, that can be divided in two populations: a small population of blue GCs, with ages between several hundred Myrs and 6 Gyrs, and one or two populations of older GCs. The first population was probably formed during the last interaction, while the second one is associated to the original galaxy. Another peculiarity of this galaxy is the distribution of GCs; Hilker & Kissler-Patig (1996) found that blue GCs are missing in a stripe extending from South-East to North of the galaxy and that red GCs are instead over-abundant in this same stripe. The inhomogeneous distribution of the HI found by Guhathakurta et al. (1990), could be the responsible of the inhomogeneous distribution of GCs, but this can not explain the overabundance of red objects in the stripe. The small amount of young GCs found in NGC 5018 ($\sim$ 10 %) is an evidence against a significant increase of GCs by a merger event for this galaxy.

NGC 5018 was also observed in the X-rays with the *Chandra X-Ray Observatory*'s Advanced CCD Imaging Spectrometer by Ghosh et al. (2005). These authors found six nonnuclear X-ray point sources in NGC 5018, as well as diffuse hot gas that may be the remnant of interactions of NGC 5018 with its neighbor galaxies. Their total absorption-corrected luminosity for the diffuse light was $13.7 \pm 1.5 \times 10^{39}$ erg/s. Ghosh et al. (2005) also estimated a radiative cooling time for the hot plasma of a few times 10^7-10^8 yr, which turns to be shorter than the age of the last interaction (Guhathakurta et al. 1990). They conclude that the gas is still falling in and that it is reheated by ionization, stellar winds, and supernovae by recent star formation activity. Moreover, they found that, even if there is little current star formation in NGC 5018, there is a significant reservoir of gas which maintains a low but steady level of star formation, also explaining the diffuse X-ray emission of the galaxy.

Recently, *Chandra* X-ray data have been analyzed by Smith et al. (2018) to study the diffuse X-ray emitting gas in major mergers. They did a rough classification of the systems in their sample into seven merger stages. According to the adopted criteria, they classify NGC 5018 as a very late stage major merger remnant.

Summarizing, our present knowledge converges in indicating that in NGC 5018 merging episode/s may have characterized its recent history. With the study of the IGL we aim at adding a new tessera in the mosaic considering its evolutionary environment.

3. OBSERVATIONS AND DATA REDUCTION

The data presented in this work are part of the VE-GAS[1] survey, which is a multiband u, g, r and i imaging survey, obtained with the ESO VLT Survey Telescope (VST).

With VEGAS we are mapping the light distribution and colors out to 8-10 Re and down to $\mu \sim$ 30 mag/arcsec^2 in the g band, for a large sample (~ 42) of early-type galaxies in different environments, including giant cD galaxies in the core of clusters. The main science goal of VEGAS are to study *i)* the galaxy structure and its faint stellar halo, including the diffuse light component, inner substructures as signatures of recent cannibalism events, inner disks and bars; *ii)* the external low-surface brightness structures of the galaxies (tidal tails, stellar streams and shells) and the connection with the environment; *iii)* for those galaxies in the sample with $D < 40$ Mpc, the GCs and galaxy satellites in the outermost regions of the host galaxy and their photometric properties (e.g. GC colours and mean GC radial colour changes). A more detailed description of the survey, the selected targets and the main scientific aims can be found in Capaccioli et al. (2015). The data reduction, performed by using the VST-Tube pipeline (Grado et al. 2012), and the analysis are described in details by Capaccioli et al. (2015); Spavone et al. (2017); Iodice et al. (2016, 2017b).

The most important step of the data processing is the estimation and subtraction of the sky background. For this reason, we adopt a *step dither* observing strategy for galaxies with large angular extent, since it allows a very accurate estimate of the sky background (Spavone et al. 2017; Iodice et al. 2016, 2017b). This strategy consists of a cycle of short exposures centered on the target and on offset fields ($\Delta \sim \pm 1$ degree). With such a technique the background can be estimated from exposures taken as close as possible, in space and time, to the scientific images. This ensures better accuracy, reducing the uncertainties at very faint surface brightness levels. This observing strategy allowed us to build an average sky background of the night, which was subtracted from each science image. This average sky frame takes into account the small contribution to the sky brightness by the smooth components plus the extragalactic background light. The residual fluctuations in the background are then estimated, and taken into account, by using the methodology described by Pohlen & Trujillo (2006), as explained in Spavone et al. (2017). These fluctuations of the sky background have been taken into

Table 1. VST exposures used in this work.

Object	Band	T_{exp} [sec]	FWHM[a] [arcsec]
NGC 5018	u	8280	0.77
	g	8280	0.77
	r	8280	0.94

[a]Median value of the FWHM.

Table 2. Basic properties of the galaxies studied in this paper.

Parameter	Value	Ref.
NGC 5018		
Morphological type	E3	RC3
R.A. (J2000)	13h13m01.0s	NED
Dec. (J2000)	-19d31m05s	NED
Helio. radial velocity	2816 km/s	NED
Distance	40.9 Mpc	Tully (1988)
NGC 5022		
Morphological type	SBb pec	RC3
R.A. (J2000)	13h13m30.8s	NED
Dec. (J2000)	-19d32m48s	NED
Helio. radial velocity	3001 km/s	NED
Distance	40.4 Mpc	NED
MCG-03-34-013		
Morphological type	S0	RC3
R.A. (J2000)	13h12m18.9s	NED
Dec. (J2000)	-19d26m46s	NED
Helio. radial velocity	2691 km/s	NED
Distance	40.7 Mpc	NED

account in the error estimates we quote on our surface brightness measurements.

In the case of NGC 5018 we adopted as offset field the one located at the West side of the galaxy (R.A. 13h08m47.260s Dec. -19d20m46.40s), since this field is not very crowded and, mainly, because it does not contain very bright galaxies and stars.

The data used in this paper consist of exposures in u, g and r bands obtained with VST + OmegaCAM, in visitor mode (run ID: 096.B-0582(B), 097.B-0806(A) and 099.B-0560(A)), during dark time, in photometric conditions, with an average seeing between 0.6 and 1.1 arcsec (see Tab. 1). In this work we analyze an area of 1.2 square degrees around NGC 5018. This area covers the three main galaxies of the small group, composed by the dominant early type galaxy, NGC 5018, the edge-on spiral, NGC 5022, the S0 galaxy MCG-03-34-013, analyzed in this work, whose main properties are listed in Tab. 2.

4. SURFACE PHOTOMETRY

4.1. *Isophotal analysis*

The isophotal analysis of the galaxies in this work is performed on the final mosaic in each band with the IRAF[2] task ELLIPSE.

In the top panel of Fig. 2 we show the VST g band image of NGC 5018, NGC 5022 and MCG-03-34-013, in surface brightness levels. In the bottom-left panel of the same figure we show the ellipticity (ϵ) and position angle (P.A.) profiles in the g band (blue points), r band (red points), and u band (green points) resulting from our isophotal analysis, performed via the ELLIPSE task as described in details in Spavone et al. (2017). The bottom-right panel shows the g, r and u band VST azimuthally averaged surface brightness profiles of NGC

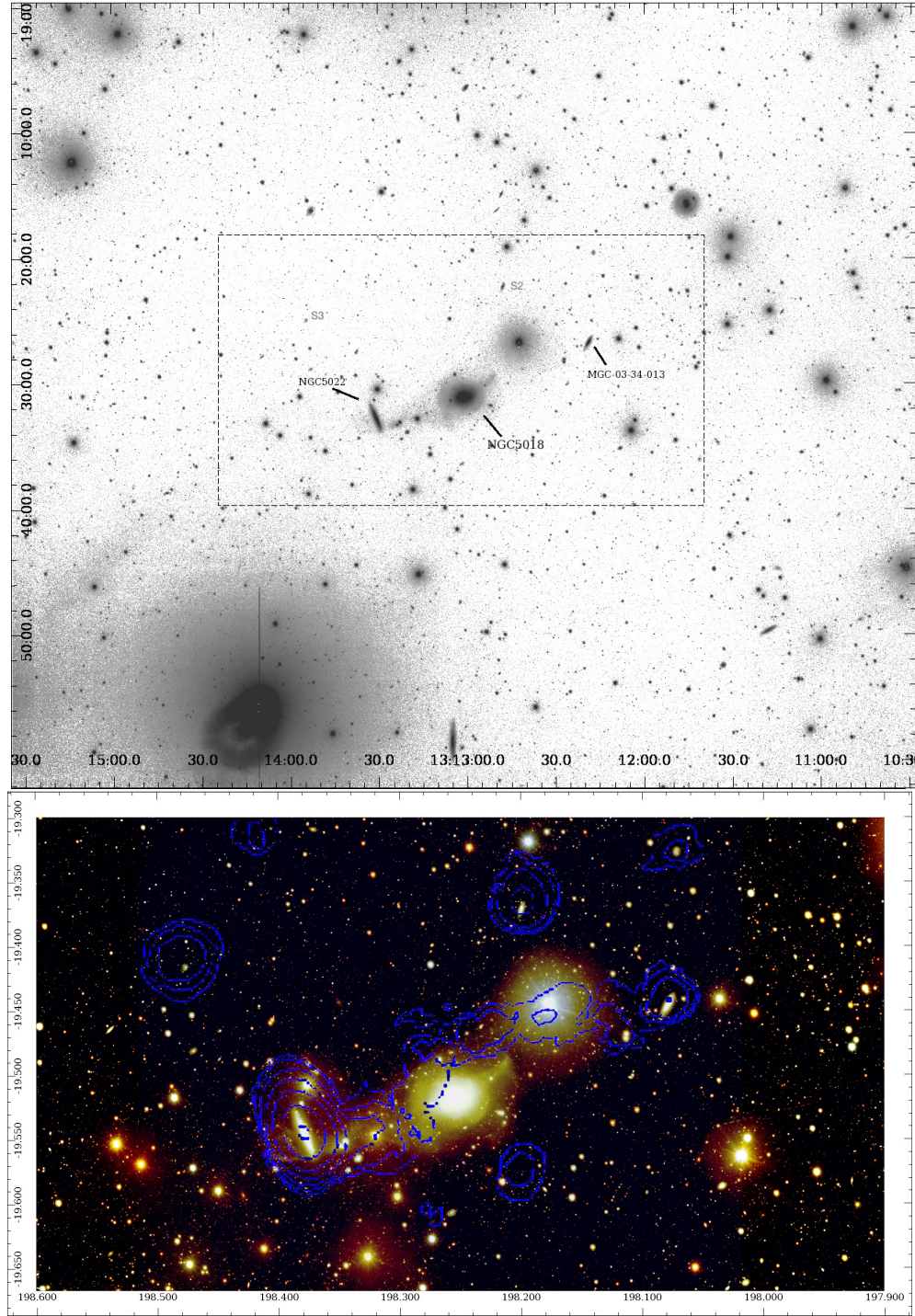5018. No correction for seeing blurring is applied to the inner regions of the profiles.

The same isophotal analysis has been performed also for NGC 5022 and MCG-03-34-013, and the results are shown in Fig. 3 and 4, respectively.

The growth curves obtained by isophote fitting, have been extrapolated to the derive total magnitudes m_T, effective radii R_e and corresponding effective magnitude μ_e in each band (Tab. 3). All the reported magnitudes are corrected for interstellar extinction, by using extinction coefficients derived by Burstein & Heiles (1982).

4.2. *Two dimensional model of the light distribution*

The IRAF task BMODEL creates a 2-dimensional image file containing a noiseless photometric model of a source image ("parent image"). The model is built from the results of isophotal analysis generated by the isophote fitting task, ELLIPSE. We use BMODEL to create a model of NGC 5018, which is able to take into account also ellipticity and P.A. variations. In Fig. 5 we show the residual image obtained by subtracting from the VST g band image the galaxy model.

The complex structure of NGC 5018 stands out very clear from the residual image. From this map, in fact, we can clearly identify a numer of substructures, such as

---

[2] IRAF (*Image Reduction and Analysis Facility*) is distributed by the National Optical Astronomy Observatories, which is operated by the Associated Universities for Research in Astronomy, Inc. under cooperative agreement with the National Science Foundation.

Figure 1. *Top*: VST g-band mosaic of NGC 5018 group. The image size is $1.2° \times 1.0°$. *Bottom*: Color composite image of the central regions of the group ($0.7° \times 0.4°$), assembled from u, g and r band VST images, with the HI map from the VLA superimposed (blue contours), adapted from Kim et al. (1988).
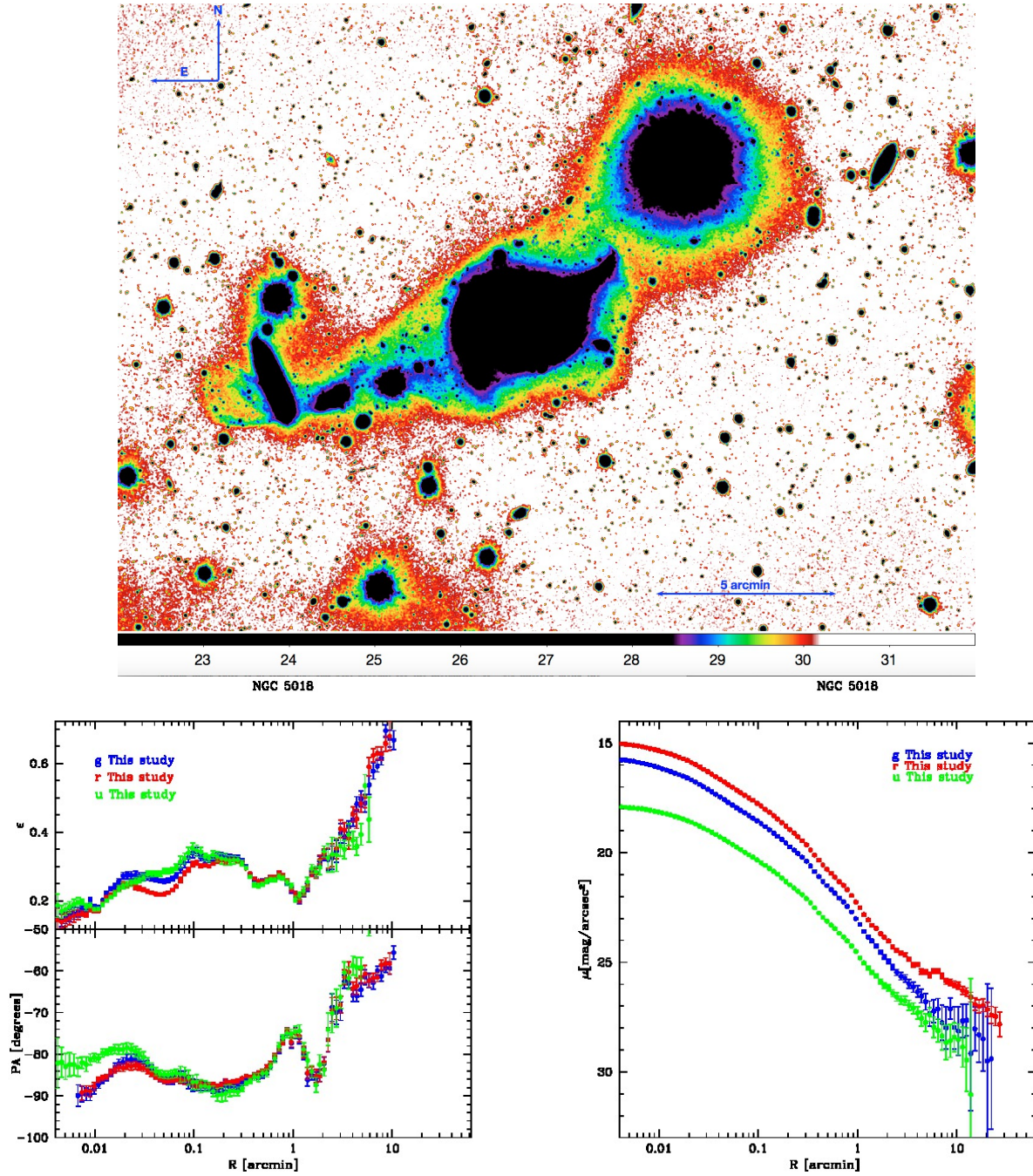
Figure 2. *Top*: VST *g* band sky-subtracted image of the $0.4° \times 0.4°$ field around NGC 5018. The color scale represents surface brightness in mag/arcsec^2. *Bottom left*: ellipticity (ϵ) and position angle (P.A.) profiles for NGC 5018, in the *g* band (blue points), *r* band (red points), and *u* band (green points). *Bottom right*: Azimuthally averaged surface brightness profiles in the *g* (blue), *r* (red), and *u* (green) bands.
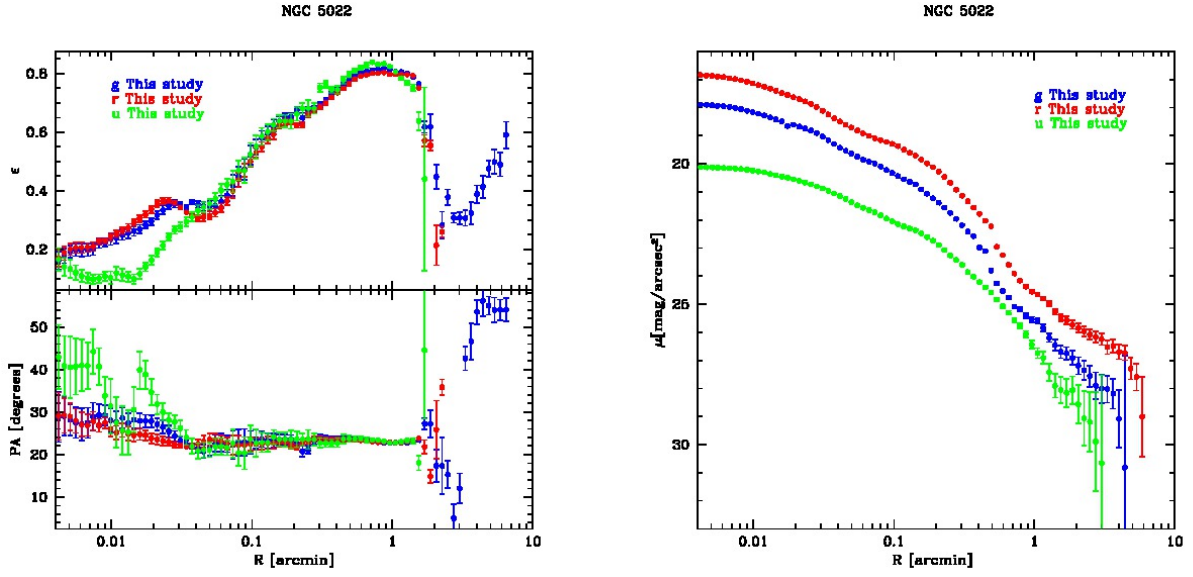
Figure 3. *Left*: ellipticity (ϵ) and position angle (P.A.) profiles for NGC 5022, in the g band (blue points), r band (red points), and u band (green points). *Right*: Azimuthally averaged surface brightness profiles in the g (blue), r (red), and u (green) bands.
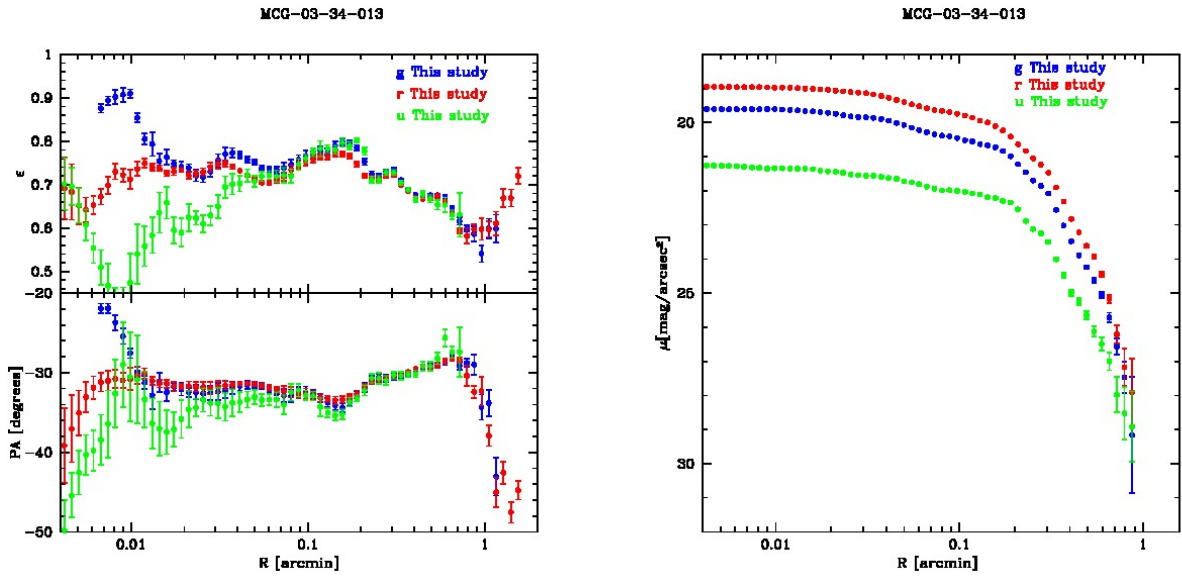
Figure 4. *Left*: ellipticity (ϵ) and position angle (P.A.) profiles for MCG-03-34-013, in the g band (blue points), r band (red points), and u band (green points). *Right*: Azimuthally averaged surface brightness profiles in the g (blue), r (red), and u (green) bands.

a prominent tail in the NW side of the galaxy, the bridge connecting NGC 5018 with NGC 5022 and the loop on the SE side of NGC 5022, which were also visible in the "parent image", as well as multiple shells, filaments and fans of stellar light, extending to the central galaxy regions.

We used the method described by Tal et al. (2009) to quantify the tidal disturbance of NGC 5018, by dividing the masked VST g band image of the galaxy and the

galaxy model obtained as explained above. The resulting model frame is shown in Fig. 6

From this figure it appears even more clearly the complex dust lanes system in the central regions of the galaxy, as well as its multiple shells and fans of diffuse material. NGC 5018, in fact, has been classified by Tal et al. (2009) as an "Highly Disturbed Galaxy", on the basis of its tidal parameter. According to these authors, such a complex system is probably the result of merg-

Table 3. Distances and photometric parameters for the sample galaxies.

Object	D [Mpc] (a)	A_u [mag] (b)	A_g [mag] (b)	A_r [mag] (b)	$\mu_{e,u}$ [mag/arcsec^2] (c)	$r_{e,u}$ [arcmin]	$m_{T,u}$ [mag] (c)	$M_{T,u}$ [mag] (c)	$\mu_{e,g}$ [mag/arcsec^2] (c)	$r_{e,g}$ [arcmin]	$m_{T,g}$ [mag] (c)	$M_{T,g}$ [mag] (c)	$\mu_{e,r}$ [mag/arcsec^2] (c)	$r_{e,r}$ [arcmin]	$m_{T,r}$ [mag] (c)	$M_{T,r}$ [mag] (c)
NGC 5018	40.9	0.493	0.362	0.263	24.98	1.40	11.71	-21.35	21.92	0.54	10.93	-22.49	24.68	3.41	9.29	-23.77
NGC 5022	40.4	0.513	0.377	0.274	23.83	0.43	14.09	-18.94	21.67	0.29	13.38	-19.65	25.47	1.89	11.93	-21.10
MCG-03-34-013	40.7	0.495	0.364	0.264	22.33	0.23	15.50	-17.55	21.05	0.22	14.19	-18.86	20.45	0.22	13.61	-19.44

[a] Distance of NGC 5018 is from Tully (1988); distances of NGC 5022 and MCG-03-34-013 are from NED.

[b] Extinction correction in the u, g and r band are from Burstein & Heiles (1982).

[c] Derived by integrating the growth curves and corrected for interstellar extinction.
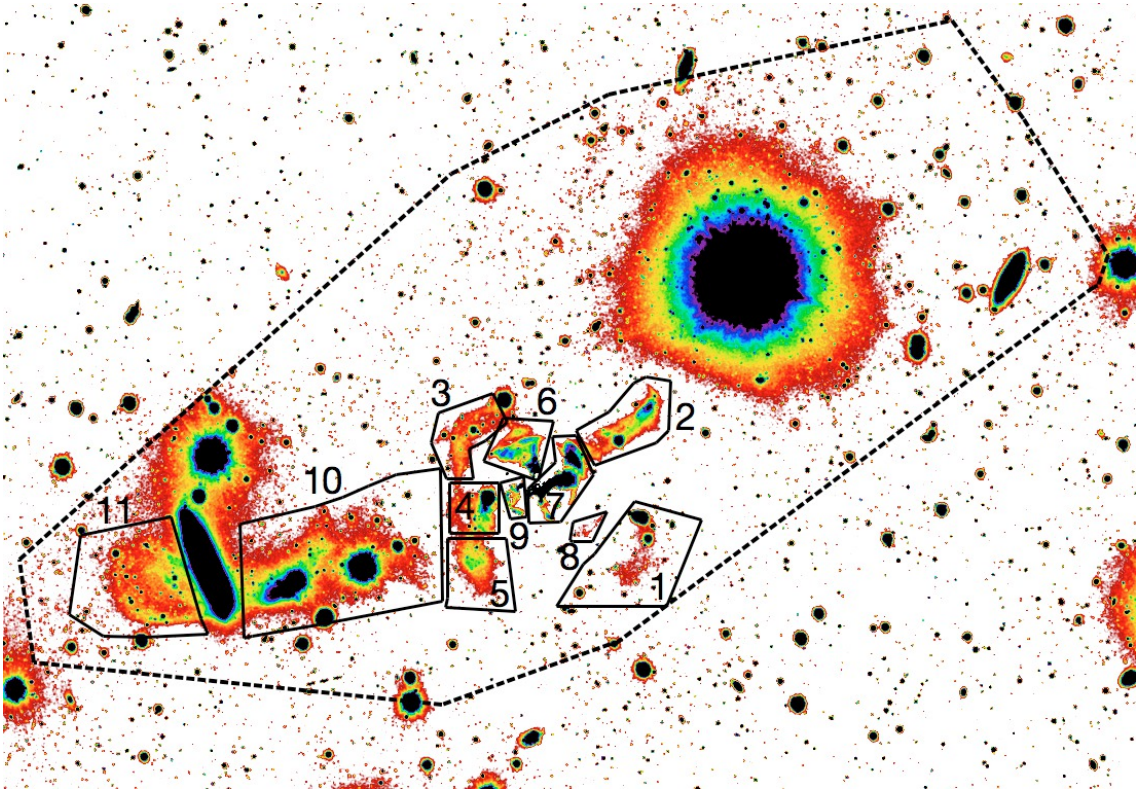
Figure 5. Residual image obtained by subtracting from the VST g band image the galaxy model. The numbers indicate the most luminous substructures for which we have estimated the integrated colors (see Sec. 4.3). The dashed polygon marks the area over which we estimated the integrated magnitudes and colors of the intra group component (see Sec. 4.4.

ers with multi-component objects such as S0 or spiral galaxies.

4.3. Color distribution

We have derived the azimuthally averaged, extinction corrected *(g - r)* and *(u - g)* color profiles (Fig. 7, bottom panel) and the 2D color maps centered on NGC 5018 (top and middle panels). On average, central regions are bluer then the outer ones, but the colors are consistent with those typically found for ETGs (La Barbera et al. 2012). From both the color maps it is evident

the complex system of dust lanes in the center of the galaxy.

Azimuthally averaged, extinction corrected, *(g - r)* and *(u - g)* color profiles have been derived also for NGC 5022 and MCG-03-34-013, and are shown in the bottom panels of Fig. 7.

By using the residual map shown in Fig. 5, we derived the integrated *(g - r)* colors in the substructures standing out from this map. To this aim, after masking all the bright sources, we define on the residual map a set of polygons covering such substructures, and used them to estimate the integrated colors, with the main goal
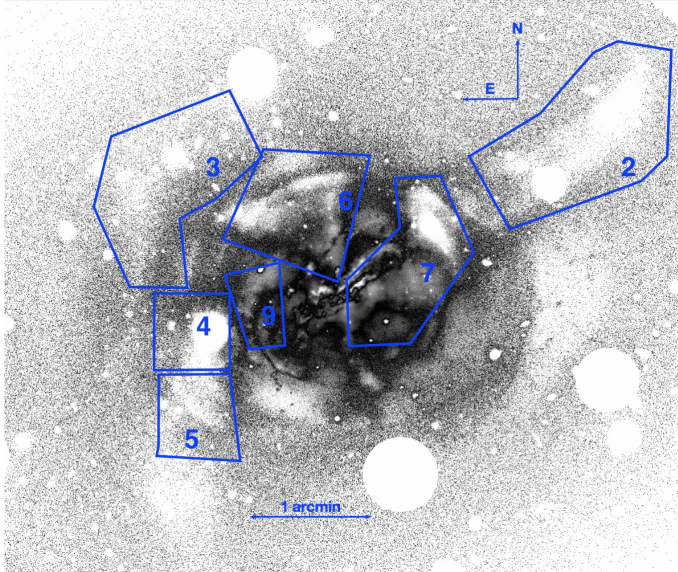
Figure 6. Result of model fitting and division method employed to quantify the tidal disturbance of NGC 5018 (see text). The image size is 6×5 arcmin. The overplotted blue contours mark the substructures shown in Fig. 5 which are also visible in this image.

to compare them with those of the galaxies belonging to the group. In Fig. 8 we show the integrated colors of the different polygons, compared with those of the galaxies ($(g\text{-}r)_{NGC5018} = 0.67 \pm 0.02$, $(g\text{-}r)_{NGC5022} = 0.73 \pm 0.02$, $(g\text{-}r)_{MCG-03-34-013} = 0.62 \pm 0.02$), marked as dashed red lines in the plot.

From this comparison, shown in Fig. 8, we can see that substructures labelled as 1 ($(g\text{-}r) = 0.97$), 5 ($(g\text{-}r) = 0.9$), 10 ($(g\text{-}r) = 1.08$), and 11 ($(g\text{-}r) = 1.1$) have colors consistent with each other, but redder than those of the galaxies in the group. This suggests that all the above features are part of a single structure, which could have an external origin, since its color is not compatible with any of the galaxy in the group. Moreover, we can note that the colors of these substructures are comparable with those of the outskirts of both NGC 5018 and NGC 5022. The implications of this result will be discussed in Sec. 8.

The colors of all the other identified substructures appear to be similar to that of NGC 5018, suggesting that they could be part of the parent galaxy.

4.4. Integrated colors of the intra group light

We used the IRAF task POLYMARK to define a region in the residual map centered on NGC 5018 (see Fig. 5) covering the bulk of intra group light (IGL). Then we use POLYPHOT to derive the integrated magnitudes in the g and r bands, and $(g - r)$ color inside this area. Foreground and background bright sources

have been masked and excluded from the estimate of the integrated quantities (see also Iodice et al. 2017b).

The extinction corrected magnitudes and color derived are $m_g^{IGL} = 11.39 \pm 0.29$ mag, $m_r^{IGL} = 10.61 \pm 0.07$ mag, and $(g - r) = 0.78 \pm 0.35$ mag, and then the total luminosity in the g band is $L_g^{IGL} = 7.06 \times 10^{10} L_\odot$. The fraction of IGL, with respect to the total luminosity of the group ($L_g = 1.7 \times 10^{11} L_\odot$) is about 41%, while with respect to the dominant galaxy NGC 5018 ($L_g = 1.5 \times 10^{11} L_\odot$) is about 47%. The integrated $(g - r)$ color of the IGL component is consistent with those of the galaxies in the group, within the errors.

Given that the IGL is composed of stars stripped from galaxies, its color relative to the galaxies can give indications on the epoch when it was stripped. In particular, if the IGL is redder than the group galaxies, it is likely that stars have been stripped from the galaxies at early times, while if the color of IGL is similar to that of galaxies, it is likely that this component have formed from the ongoing stripping of stars (Krick et al. 2006).

The ongoing stripping scenario is consistent with our results. Moreover, the color of the IGL component is also roughly consistent, within the errors, with the color of the outskirts of NGC 5018. Simulations by Willman et al. (2004) predict that ∼ 50% of intragroup stars come from bright galaxies, and as a consequence the color of the intragroup stars should be consistent with the color of the outskirts of bright group galaxies.

5. INFRARED ANALYSIS

As shown in the previous sections, the photometric analysis in the optical bands has shown the presence of a prominent and complex system of dust lanes crossing the central regions of NGC 5018. Since the dust optical depth decreases toward longer wavelengths, near-infrared (NIR) photometry can help to reduce the dust absorption, that strongly affects the starlight distribution in the galaxy. Moreover, adding some infrared bands to the photometric analysis could help to better understand the nature of the bridge connecting NGC 5018 to NGC 5022.

In this work we use images obtained with the Wide-field Infrared Survey Explorer (WISE, Wright et al. 2010) in the $w1$ (3.368 μm) and $w2$ (4.618 μm) bands, to perform the infrared photometric analysis for NGC 5018. The results of this analysis are shown in Fig. 9, where we plot the ϵ and $P.A.$ profiles (top panel), the azimuthally averaged surface brightness profiles (middle panel), and the mean $(w1 - w2)$ color profile (bottom panel).

In order to better constrain the nature of the substructures observed in the optical residual map of NGC
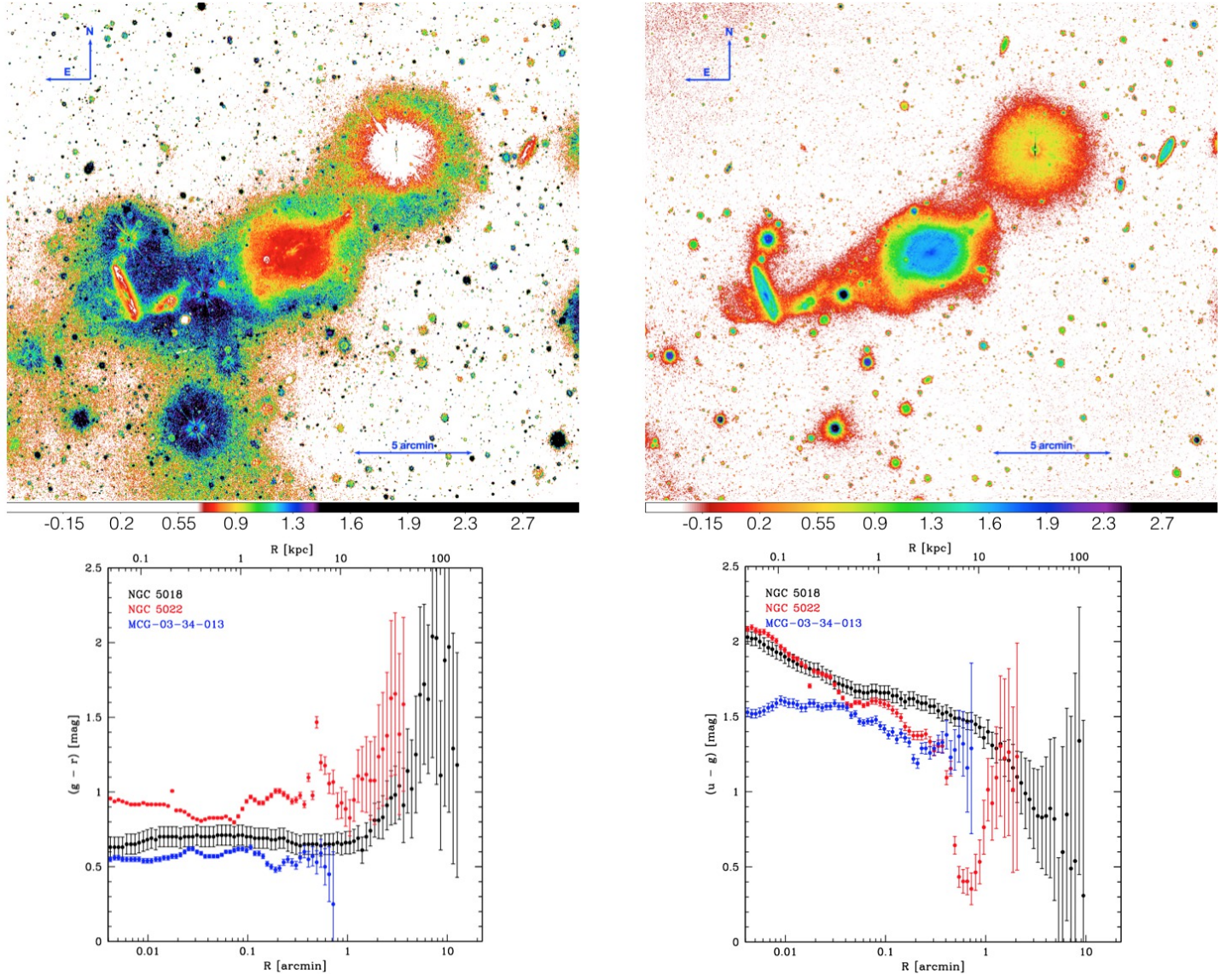
Figure 7. *(g - r)* (*Top-left panel*) and *(u - g)* (*Top-right panel*) color maps centered on NGC 5018. *Bottom*: Azimuthally averaged, extinction corrected, *(g - r)* (left) and *(u - g)* (right) color profiles of NGC 5018 (black), NGC 5022 (red) and MCG-03-34-013 (blue).

5018, we applied the same procedure described in Sec. 4.3 to the NIR residual map. We used the same polygons obtained above (see Fig. 5), to estimate the integrated NIR color of the substructure standing out form the map. We also derived the integrated colors for NGC 5018 (*(w1-w2)*=0.02), NGC 5022 (*(w1-w2)*=0.05), and MCG-03-34-013 (*(w1-w2)*=-0.01), in order to compare them with the colors of the different substructures. The results are shown in Fig. 10, where we plot the infrared colors of the different substructures compared with those of the three galaxies of the group.

This analysis confirms that also the NIR colors of the substructures number 1 (*(w1-w2)*=0.1), number 5 (*(w1-w2)*=0.09), as well as the bridge (labelled as 10,

(*(w1-w2)*=-0.06)) and the loop (labelled as 11, (*(w1-w2)*=0.22)) are not consistent with any of the galaxies in the group, as already found from the optical colors.

6. ULTRAVIOLET ANALYSIS FOR NGC 5022

In order to detect the presence of hot and young stars in the NGC 5018 group, we also performed a photometric analysis in the ultraviolet (UV) bands. The near-ultraviolet (NUV) profile of NGC 5018 has been published by Rampazzo et al. (2007), while the far-ultraviolet (FUV) profile is not published because of the low S/N in the FUV band.

The FUV and NUV images of NGC 5022 used here, were obtained from GALEX archive (see Martin et al.
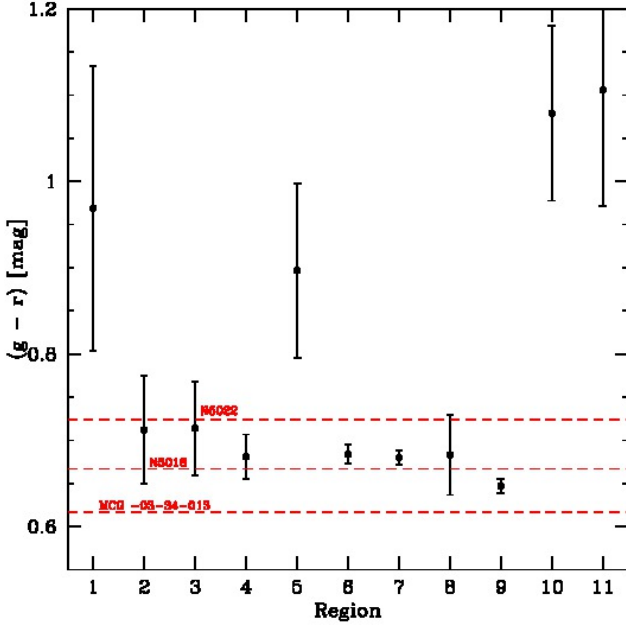
Figure 8. Integrated *(g - r)* colors in the 11 regions marked on the residual image, Fig. 5. Red dashed lines represent the integrated colors of the three main galaxies in the VST field (see Fig. 1): NGC 5018, NGC 5022 and MCG-03-34-013.

2005; Morrissey et al. 2005). The exposure times were 4451 sec in NUV and 1568 sec in FUV bands (limiting magnitude in FUV/NUV $\sim$ 22.6/22.7 AB mag Bianchi 2009).

We used FUV and NUV background-subtracted, intensity images derived from the GALEX pipeline. FUV and NUV magnitudes have been computed as $m(AB)_{UV}$ = -2.5 $\times$ log CR_{UV} +ZP, where CR is the dead-time-corrected, flat-fielded count rate and the zero points are ZP = 18.82 and ZP = 20.08 in the FUV and NUV respectively (Morrissey et al. 2007).

Both FUV and NUV surface photometry have been performed using the IRAF STSDAS ELLIPSE routine. The resulting SB profiles are shown in Fig. 11. Our measured NUV and FUV total magnitudes (NUV=16.6 $\pm$ 0.03 and FUV=17.4 $\pm$ 0.07) are consistent within errors with the one measured GALEX General Release 6. Both luminosity profiles are well fitted by a disk with n=0.9 (see the bottom panel of Fig. 11).

As for the optical images we used the IRAF task BMODEL to create a 2-D image and then we subtract this model to the origin one. The residual images are shown in Fig. 12. As we can see in the final images (right panels) are well visible three bright regions in the southern part of the disk. We suspect these are region of star formation. For this reason we measured the flux
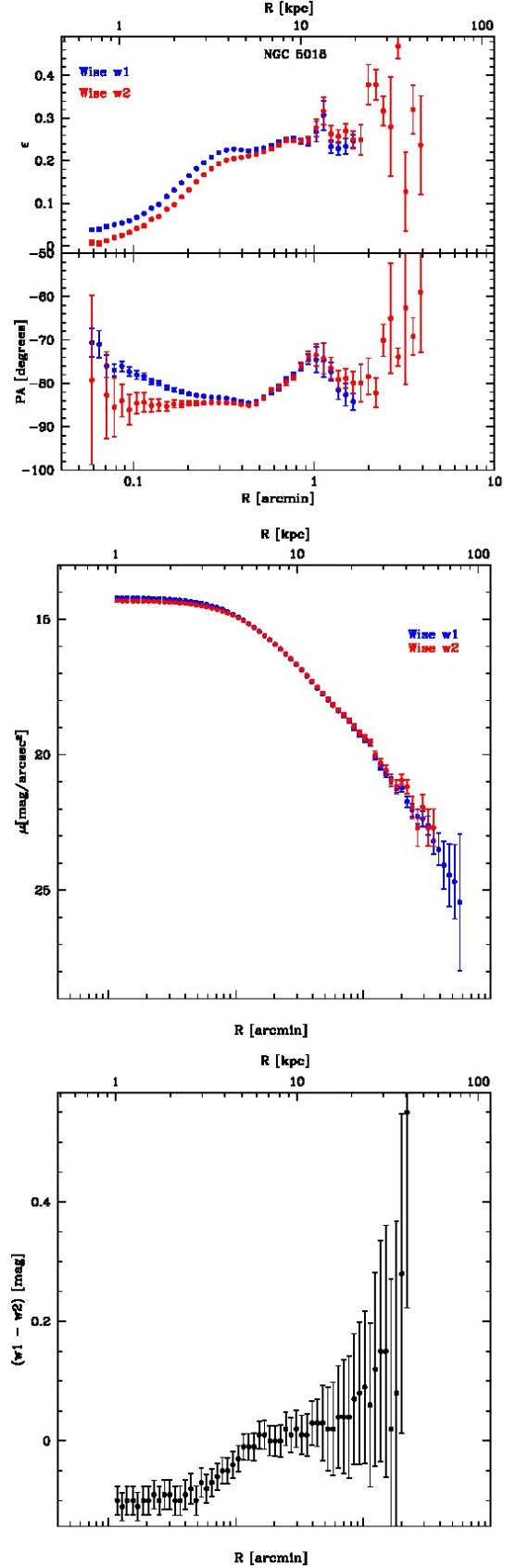
Figure 9. *Top*: ellipticity (ϵ) and position angle (P.A.) profiles for NGC 5018, in the Wise *w1* (3.368 μm, blue points) and *w2* (4.618 μm, red points) bands. *Middle*: Azimuthally averaged surface brightness profiles in the *w1* (3.368 μm, blue points) and *w2* (4.618 μm, red points) bands. *Bottom*: Azimuthally averaged color profile.
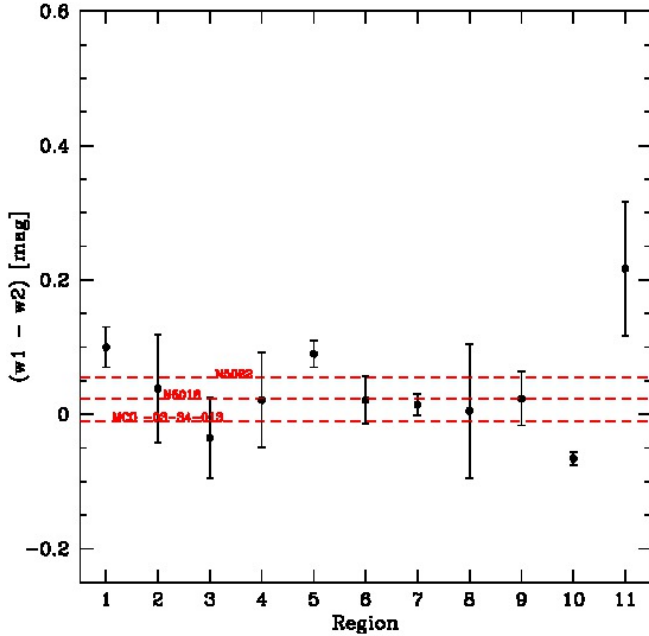
Figure 10. The same as Fig. 8 for the Wise *w1* band.

of the three blobs visible. As a comparison we measured the total NUV and FUV fluxes for the whole north part of the galaxy.

Using the FUV flux we derived the present-day Star Formation Rate (SFR) of each UV-bright blob (see the bottom-right panel of Fig. 12) following Kennicutt (1998), using its UV continuum luminosity and the relation SFR $(M_\odot/yr) = 1.4 \times 10^{-28}$ L_{FUV} (erg/s/Hz). The final results are reported in Tab. 4. As we can see the SFR is the same in all the galaxy.

7. TOTAL ACCRETED MASS IN A LOOSE GROUP OF GALAXIES

Following the procedure adopted by Spavone et al. (2017), in order to define the different components dominating the galaxies light distribution at different scales, we have described the surface brightness profiles of NGC 5018 with a three component model: a Sérsic profile (Sérsic 1963; Caon et al. 1993) for the centrally concentrated in situ stars, a second Sérsic for the "relaxed" accreted component, and another Sérsic component for the diffuse and "unrelaxed" outer envelope (Seigar et al. 2007; Donzelli et al. 2011; Arnaboldi et al. 2012; Cooper et al. 2015; Iodice et al. 2016; Spavone et al. 2017).

The stellar population of the central in situ component is expected to be similar to the dominant "relaxed" accreted component, while the outer diffuse component representing "unrelaxed" accreted material ('streams' and other coherent concentrations of debris) does not
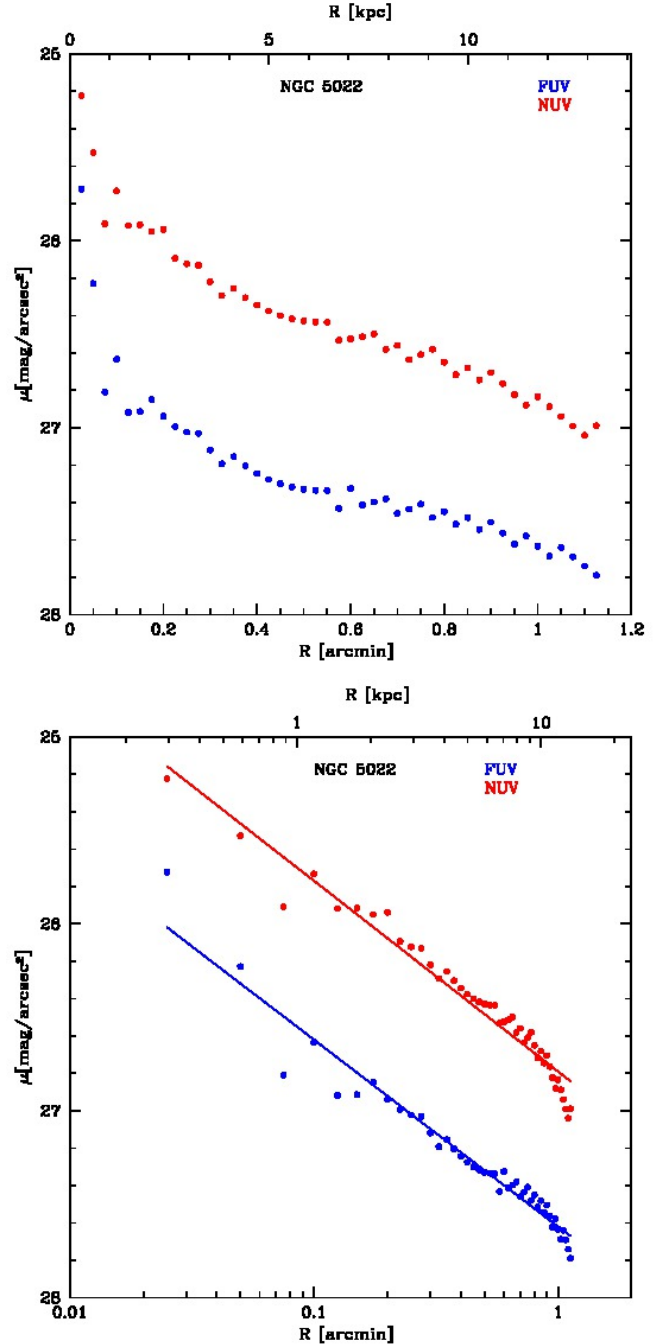

Figure 11. *Top*: Azimuthally averaged surface brightness profiles in the FUV (blue points) and NUV (red points) bands. *Bottom*: The same profiles plotted in logarithmic scale.

contribute significantly to the brighter regions of the galaxy.

For the central ETG, NGC 5018, we used the same fitting procedure described in Spavone et al. (2017), consisting in fixing $n \sim 2$ for the in situ component of our three-component fit, in order to mitigate the degeneracy
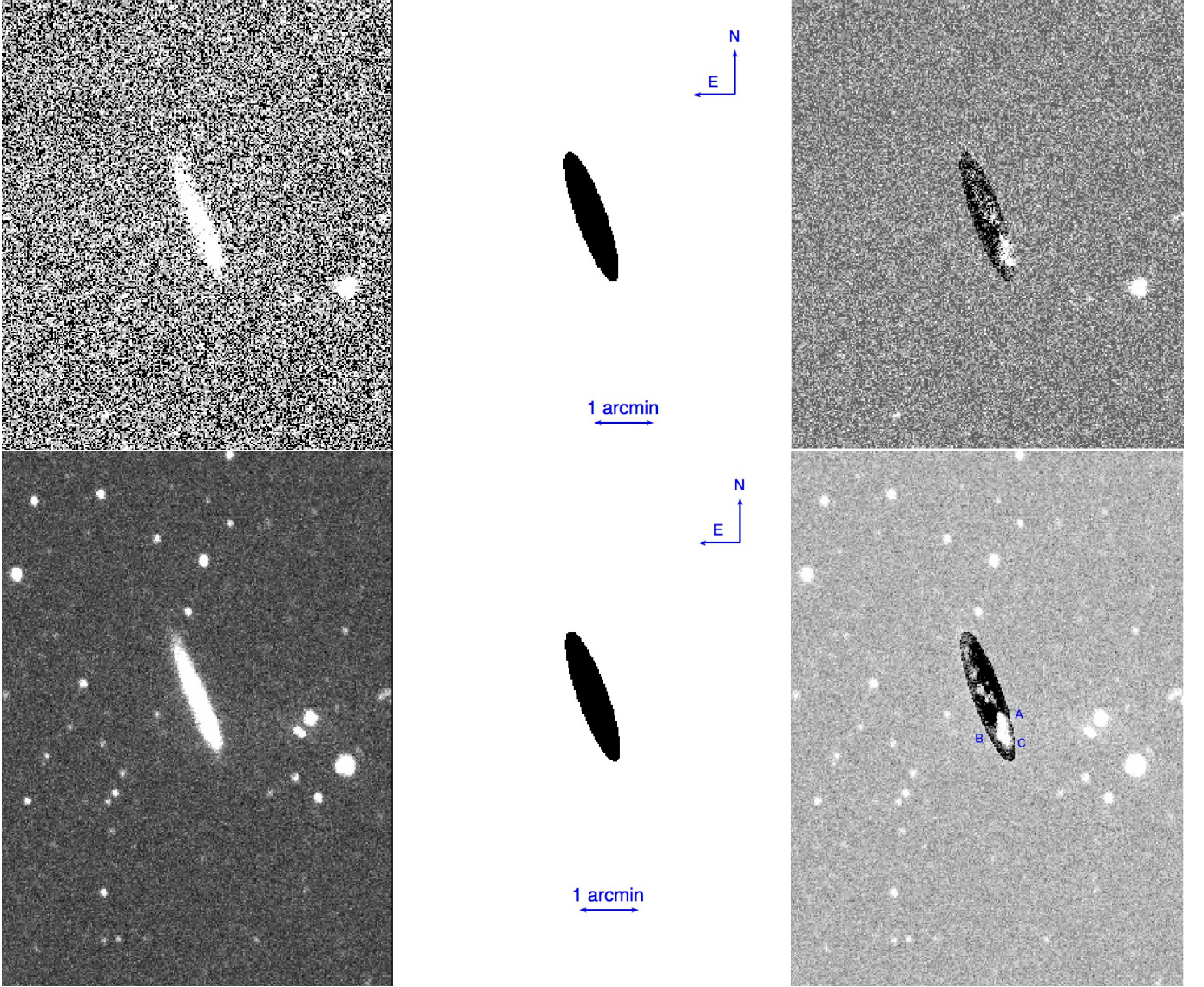
Figure 12. *Top*: FUV image of NGC 5022 (left), 2D model of the galaxy (middle), residual of the subtraction of the model (right). *Bottom*: NUV image of NGC 5022 (left), 2D model of the galaxy (middle), residual of the subtraction of the model (right).

Table 4. Integrated photometric UV properties

Object	R.A. (2000)	DEC (2000)	m_{FUV}(AB)	F_{FUV}	L_{FUV}	m_{NUV}(AB)	F_{NUV}	L_{NUV}	FUV-NUV	SFR_{FUV}
Galaxy	198.38	-19.54	17.4±0.07	1.84	4.08	16.6±0.03	1.27	2.82	0.8	5.7
A	198.373	-19.5578	18.42±0.19	0.75	1.64	17.64±0.21	0.65	1.44	0.92	2.32
B	198.3748	-19.5563	17.86±0.14	1.13	2.5	17.5±0.11	0.74	1.64	0.59	3.5
C	198.3741	-19.5528	18.02±0.09	0.98	2.18	17.27±0.08	1.00	2.22	0.75	3.05

Notes: (1) Coordinates are given in degrees. (2) Fluxes are in units of 10^{-27} erg s^{-1}cm$^{-2}Hz^{-1}$. (3) Luminosities are in units of 10^{26} erg s^{-1} Hz^{-1}. (4) SFRs are in units of 10^{-2} M$_\odot$ yr^{-1}

in parameters in such kind of fit. This typical value of n has been adopted on the basis of the results of Cooper et al. (2013) for massive galaxies. The results of this fit for NGC 5018, with the corresponding (O-C) residuals, are shown in Fig. 13, both in logarithmic (top panel) and in linear (bottom panel) scale, while the best-fitting structural parameters for the fit are reported in Tab. 5. The result of the fit show that the outer part of this galaxy's surface brightness profile is almost exponential in nature, and in fact we checked that fitting an outer exponential component to the surface brightness profile, does not change the residuals and the shape of the total fitted profile.

The surface brightness profiles of NGC 5022 and MCG-03-34-013 have also been fitted with a three and two component model, respectively, in which all the parameter were left free. The results of the fit are shown in Fig. 14 and the best-fitting parameters are reported in Tab. 5.

We used these fits to derive the total magnitude of the different Sérsic components, $m_{T,1}$, $m_{T,2}$, and $m_{T,3}$, as well as the relative contribution of the accreted component with respect to the total galaxy light, $f_{h,T}$, reported in Tab. 5. The total accreted mass fraction for the galaxies in this small group, ranges between 78% and 92%. These values are consistent with the results of numerical simulations, which predict that stars accreted by BCGs account for most of the total galaxy stellar mass (Cooper et al. 2013, 2015; Pillepich et al. 2018).

These results can be used to estimate the stellar mass fractions in the different components by assuming appropriate stellar mass-to-light ratios, in order to compare the accreted mass ratios we infer from our observations with other observational estimates for BCGs of similar total mass by Seigar et al. (2007); Bender et al. (2015); Iodice et al. (2016); Spavone et al. (2017), and with theoretical predictions from semi-analytic particle-tagging simulations by Cooper et al. (2013, 2015), and the Illustris cosmological hydrodynamical simulations (Pillepich et al. 2018).

To this aim, we measured the mean (u - g) and (g - r) colors for each galaxy in regions where the central galaxies and the outer envelopes dominate, obtaining the values reported in Tab. 6. We then used stellar population synthesis models (Vazdekis et al. 2012; Ricciardelli et al. 2012), with a Kroupa IMF, to derive the mass-to-light ratios corresponding to the average colors, and hence the stellar mass of the whole galaxy and of the outer envelope. These results are summarized in Table 6 and the comparison is shown in Fig. 15. Since simulations used to compare the stellar halo mass frac-
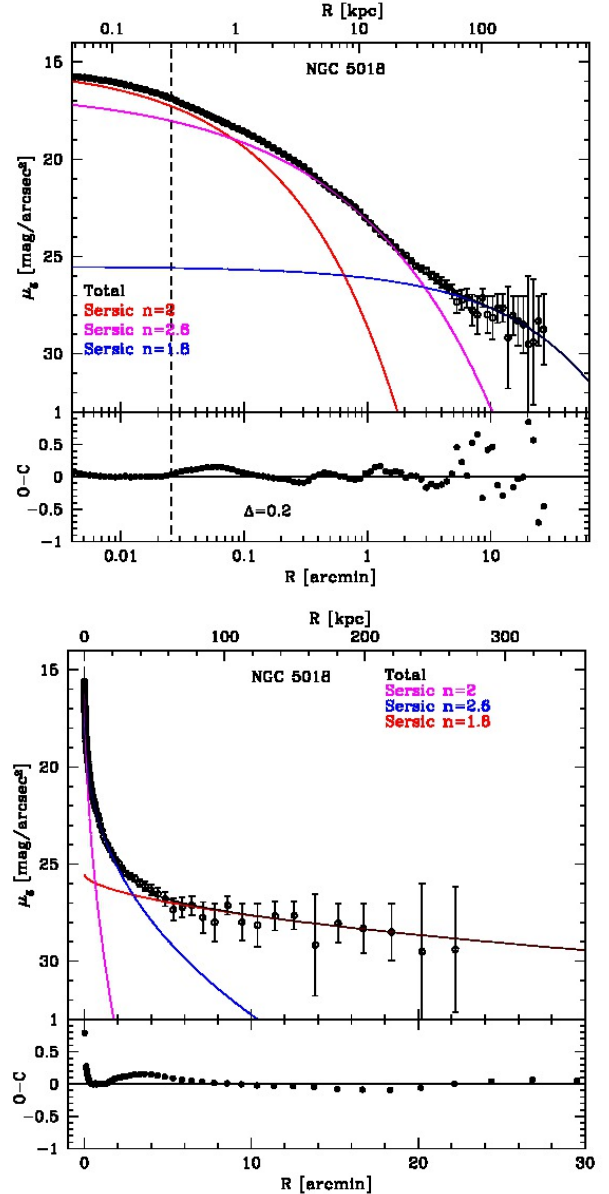
Figure 13. VST g band profile of NGC 5018, in logarithmic (top) and linear (bottom) scale, fitted with a three component model motivated by the predictions of theoretical simulations (see Spavone et al. (2017)).

tion of our galaxies cover scales from the stellar haloes of Milky Way-like galaxies to the cD envelopes of groups and clusters. For this reason the comparison shown in the Fig. 15 is meaningful only for the more massive galaxy of the group.

We find that the stellar mass fraction of the accreted component derived for the three main galaxies in the NGC 5018 group is fully consistent both with published data for other BCGs (Seigar et al. 2007; Bender et al. 2015; Iodice et al. 2016; Spavone et al. 2017), de-

Table 5. Best-fitting structural parameters for a three-component fit.

Object	μ_{e1} [mag/arcsec^2]	r_{e1} [arcsec]	n_1	μ_{e2} [mag/arcsec^2]	r_{e2} [arcsec]	n_2	μ_{e3} [mag/arcsec^2]	r_{e3} [arcsec]	n_3	$m_{T,1}$ [mag]	$m_{T,2}$ [mag]	$m_{T,3}$ [mag]	$f_{h,T}$
NGC 5018	19.10±0.10	5.24±0.07	2	21.67 ±0.34	31.75±0.50	2.6±0.1	29.06±0.20	1502±7	1.8±0.2	12.16	10.77	9.79	92%
NGC 5022	20.15±0.50	3.00±0.20	1.26±0.35	21.55 ±1.27	12.27±2.90	0.60±0.20	26.38±0.32	87.61±7.6	3.00±0.62	14.38	12.72	13.28	88%
MCG-03-34-013	21.70±0.06	12.09±2.00	0.50±0.34	22.18 ±0.18	11.55±0.02	1.25±0.03	-	-	-	12.16	10.77	-	78%

Note—Columns 2, 3, and 4 report effective magnitude and effective radius for the inner component of each fit. The Sérsic index for the in situ component of the BCG NGC 5018 was fixed to $n \sim 2$ using the models as a prior (Cooper et al. 2013), as explained in Spavone et al. (2017). We allowed small variations of ±0.5 around the mean value of $n = 2$. This would bracket the range of n in the simulations and allows us to obtain a better fit. Columns 5, 6, 7, 8, 9 and 10 list the same parameters for the second and the third components. Columns 11, 12, and 13 report the total magnitude of the inner ($m_{T,1}$) and outer Sérsic components ($m_{T,2}$ and $m_{T,3}$). Column 14 gives the total accreted mass fraction derived from our fit.

Table 6. Total and accreted stellar masses of galaxies in our sample.

Object	$(u-g)$ [mag]	$(g-r)$ [mag]	$(M/L)_g$ [$M_\odot/L_\odot$]	M^*_{tot} [$M_\odot$]	$M^*_{total\ accreted}$ [$M_\odot$]
NGC 5018	1.6 ± 0.4	0.7 ± 0.2	1.97	2.9×10^{11}	2.7×10^{11}
NGC 5022	1.0 ± 0.4	1.6 ± 0.5	1.48	1.6×10^{10}	1.4×10^{10}
MCG-03-34-013	0.6 ± 0.1	1.4 ± 0.1	0.82	4.3×10^{9}	3.3×10^{9}

Note—Columns 2, 3 and 4 show the mean, extinction corrected, u - g and g-r colours of each galaxy and the relative mass-to-light ratios in the g band. Columns 5 is the galaxy stellar mass, while column 6 reports the total accreted stellar masses, derived from the three and two-component fit.

spite considerable differences in the techniques and assumptions involved, and with the theoretical models by Cooper et al. (2013, 2015) and by Pillepich et al. (2018).

8. DISCUSSION AND CONCLUSIONS

In this work we present a new deep mosaic of 1.2×1.0 square degrees of the group of galaxies centered on NGC 5018, acquired at the ESO VLT Survey Telescope. Taking advantage of the deep and multiband photometry (in u, g, r bands) and of the large field of view of the VST telescope, we studied the structure of the galaxy members and the faint feature into the intra-group space and, then, we give an estimate of the intragroup diffuse light in the NGC 5018 group of galaxies.

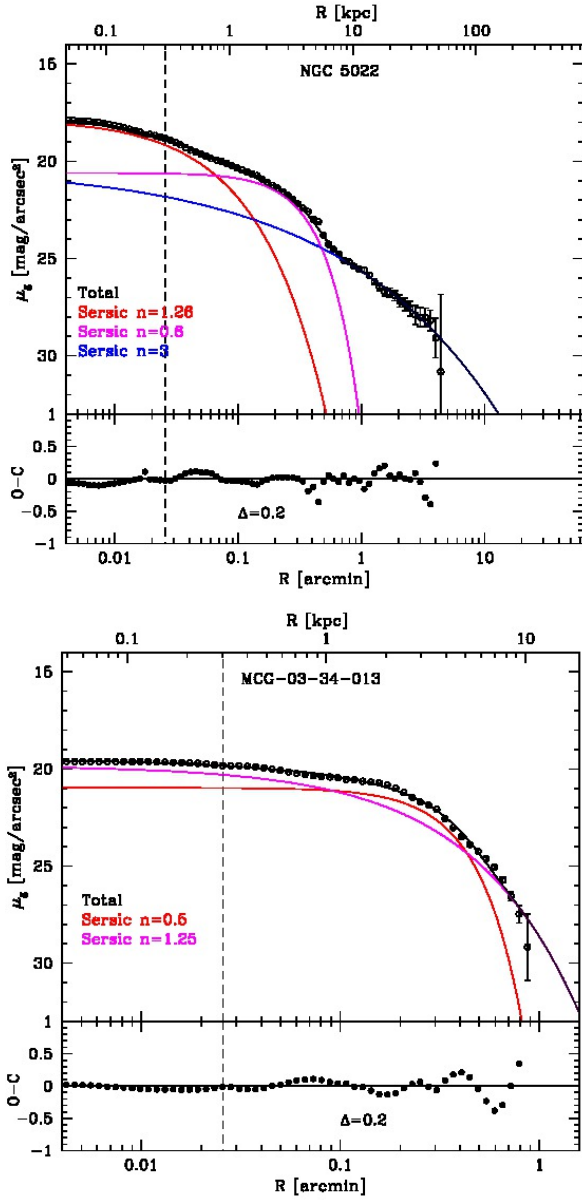### 8.1. *Tracing the build-up history of the group*

NGC 5018, sometimes classified as E3, and at South-East NGC 5022 which is an edge-on spiral, seem to be linked by a very low surface brightness filament. Indeed, many sources in the literature identify these two as an interacting pair of galaxies.

The spiral at South-East shows no warp or obvious signs of interaction, while N5018 exhibits a perturbed morphology in the outskirts, with shells and ripples, as well as inner dust signs. The HI map from the VLA (Fig. 1) indicates that there is a long tail of gas that connects NGC 5022 to the another group member, MCG-03-34-013, on the North-West with respect to NGC 5018. Such a HI filament is on the north and does not crosses NGC 5018, although a branch of it does enter the galaxy. Therefore, one open issue in the formation history of the group is if the tails and all intra-group features visible in the light distribution are tracing the same interaction traced by the cold gas filaments.
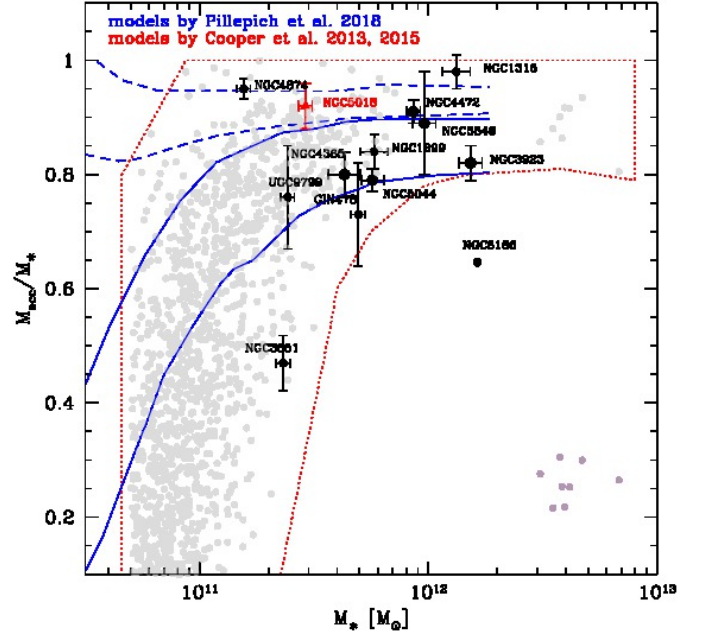
Taking advantage by the multi-band observations from VEGAS, we are able to estimate the integrated colors of all the intra-group features (see Sec. 4.4). We found that the integrated optical colors of all substructures (see Fig. 5), are not consistent with the average colors of any of the galaxies in the group, being redder. This is confirmed by estimating the NIR integrated colors for the same regions and galaxies. Therefore, this finding suggests an external origin for them.

Something similar was found for the bright galaxy NGC 1316, in SW subgroup of the Fornax cluster (Iodice et al. 2017a), where, by adopting the same approach based on the color analysis, authors concluded that some of the substructures in the envelope come from a recent accretion event of smaller and bluer galaxy, while large and redder tidal tail are more reasonably related to an earlier interaction event.

Figure 15. Accreted mass fraction vs. total stellar mass for ETGs. The measurement for NGC 5018 is given as red triangle. Black circles correspond to other BCGs from the literature (Seigar et al. 2007; Bender et al. 2015; Iodice et al. 2016; Spavone et al. 2017). Red region indicates the predictions of cosmological galaxy formation simulations by Cooper et al. (2013, 2015). Blue continuous and dashed regions indicate the accreted mass fraction measured within 30 kpc and outside 100 kpc, respectively, in Illustris simulations by Pillepich et al. 2018 (see their Fig. 12). Purple-grey points show the mass fraction associated with the streams from Tab. 1 in Cooper et al. (2015).

Figure 14. VST g band profiles of NGC 5022 (top), fitted with a three components model, and MCG-03-34-013 (bottom), fitted with a double Sersic model.

In NGC 5018, the analysis of the integrated colors suggests that the plume at the NW side and all the substructures in its central spheroid, are coeval with the galaxy, given that they have comparable colors. These features can thus be interpreted as material expelled from NGC 5018 during a merging event in its formation history. Differently, the bridge between NGC 5018 and NGC 5022, the diffuse loop on the est side of NGC 5022, and the patches numbered as 1 and 5 on East and SW side (see Fig.5), have both optical and NIR colors not consistent with the average colors of any of the galaxies in the group, which are in the range $g - r \sim 0.6 - 0.75$ mag, being redder ($g - r \sim 0.9 - 1.1$ mag, see Fig.8). They are more similar to the colors in the outskirts of NGC 5018 and NGC 5022, which are $g - r \sim 0.9 - 1.4$ mag for $1 \leq R \leq 4$ arcmin (see Fig.7). Therefore, we claim that such a features could be made by a stripped material from the galaxy outskirt in a close passage. In particular, the almost polar half-ring on the East side of NGC 5022 could formed by the interaction with an high inclined orbit (see e.g. Bournaud & Combes 2003). Moreover, such an interaction might have triggered the new star formation regions in the south part of NGC 5022, as found from the analysis of the UV data (see Sec. 6).

On the other hand, the long tail of HI gas is tracing the interaction between NGC 5022 and MCG-03-34-013 (see also Kim et al. 1988; Guhathakurta et al. 1990).

8.2. *Total accreted mass and intra-group light estimates*

According to Spavone et al. (2017), by fitting the SB profile of NGC 5018 with three Sérsic components, we were able to have an estimate of the total accreted mass in this galaxy, which is the brightest group member, and for all the less brighter galaxies (see Sec.7). We found that the total accreted mass fraction for the galaxies in this small group, ranges between 78% and 92%. These values are consistent with the results of numerical simulations by Cooper et al. (2013, 2015); Pillepich et al. (2018) and with published data for other BCGs (Seigar et al. 2007; Bender et al. 2015; Iodice et al. 2016; Spavone et al. 2017), despite considerable differences in the techniques and assumptions involved (see Fig.15).

The change in the trend of the ellipticity and P.A. with radius appears to correlate with an inflection in the SB profile of NGC 5018, which also marks the transition between the two accreted components in the fit of the light distribution (see Fig. 13). As already pointed out in Spavone et al. (2017), such inflection could mark the transition between two components in different states of dynamical relaxation. The upward inflection of the profile over the transition radius, occurs well beyond $2R_e$, suggesting an excess of weakly-bound stars associated with a recent accretion event. NGC 5018 shows clear signs of ongoing interaction and accretion events, indicating that its outer regions are still being assembled, consistent with theoretical expectations for such galaxies (e.g. Cooper et al. 2015).

The total g-band luminosity of the IGL is $L_g^{IGL} = 7.06 \times 10^{10} L_\odot$, which is $\sim 41\%$ of the total luminosity of the group. The IGL has $(g$ - $r) = 0.78 \pm 0.35$ mag, which is similar to the color in the halo of the BCG in the group core, NGC 5018, and consistent with the integrated colors of the other galaxies in the group. This is consistent with that found in many compact group of galaxies (Da Rocha & Mendes de Oliveira 2005; White et al. 2003; Da Rocha et al. 2008), and with the prediction of numerical simulations (Sommer-Larsen 2006). The presence of IGL indicates that tidal encounters stripped a considerable amount of mass from the member galaxies, and that the group is in an advanced stage of its dynamical evolution (Da Rocha & Mendes de Oliveira 2005; Sommer-Larsen 2006; Rudick et al. 2006). Slow encounters in group environment are in fact effective in liberating stars in the intragroup medium, and since the fraction of IGL increases with the degree of dynamical evolution of the group/cluster, it can be used as a "dynamical clock": more evolved groups/clusters have largest fractions of diffuse light.

Moreover, as already argued by Krick & Bernstein (2007), the color of IGL and its correlation with the color of galaxies in the group, could help to constrain the epoch at which stars forming the IGL have been stripped. In the case of NGC 5018, since the color of the IGL component is consistent with those of galaxies belonging to the group, the ongoing stripping scenario is the most plausible for the formation of intragroup light in this system.

As a conclusive remark, the picture emerging from the multi-wavelength study illustrated in this work is that there are at least two different interactions involving the group members: one between the two brightest galaxies NGC 5018 and NGC 5022, which generates the tails and ring-like structures detected in the light, and another between the two gas-rich galaxies of the group, NGC 5022 and MCG-03-34-013 that have produced the long HI tail connecting the two systems. Moreover, a minor merging event also happened in the formation history of NGC 5018 that have perturbed the inner structure of this galaxy.

The unperturbed isophotes of MCG-03-34-013 would suggest that the interaction involving such a small galaxy with NGC 5022 is more likely an high-velocity encounter between them, while the gravitational forces between the two bright group members were strong enough to perturb the outskirts and generate intragroup material.

REFERENCES

Aguerri, J. A. L., Gerhard, O. E., Arnaboldi, M., et al. 2005, AJ, 129, 2585

Aguerri, J. A. L., Castro-Rodríguez, N., Napolitano, N., Arnaboldi, M., & Gerhard, O. 2006, A&A, 457, 771

Arnaboldi, M., Aguerri, J. A. L., Napolitano, N. R., et al. 2002, AJ, 123, 760

Arnaboldi, M., Gerhard, O., Aguerri, J. A. L., et al. 2004, ApJL, 614, L33

Arnaboldi, M., Ventimiglia, G., Iodice, E., Gerhard, O., & Coccato, L. 2012, A&A, 545, AA37

Bender, R., Kormendy, J., Cornell, M. E., & Fisher, D. B. 2015, ApJ, 807, 56

Bertola, F., Burstein, D., & Buson, L. M. 1993, ApJ, 403, 573

Bianchi, L. 2009, Ap&SS, 320, 11

Bournaud, F., & Combes, F. 2003, A&A, 401, 817

Burstein, D., & Heiles, C. 1982, AJ, 87, 1165

Buson, L. M., Bertola, F., Bressan, A., Burstein, D., & Cappellari, M. 2004, A&A, 423, 965

Cantiello, M., D'Abrusco, R., Spavone, M., et al. 2018, A&A, 611, A93

Caon, N., Capaccioli, M., & D'Onofrio, M. 1993, MNRAS, 265, 1013

Capaccioli, M., Spavone, M., Grado, A., et al. 2015, A&A, 581, A10

Carollo, C. M., & Danziger, I. J. 1994, MNRAS, 270, 743

Castro-Rodríguez, N., Aguerri, J. A. L., Arnaboldi, M., et al. 2003, A&A, 405, 803

Castro-Rodriguéz, N., Arnaboldi, M., Aguerri, J. A. L., et al. 2009, A&A, 507, 621

Contini, E., De Lucia, G., Villalobos, Á., & Borgani, S. 2014, MNRAS, 437, 3787

Cooper, A. P., Cole, S., Frenk, C. S., et al. 2010, MNRAS, 406, 744

Cooper, A. P., D'Souza, R., Kauffmann, G., et al. 2013, MNRAS, 434, 3348

Cooper, A. P., Gao, L., Guo, Q., et al. 2015, MNRAS, 451, 2703

D'Abrusco, R., Cantiello, M., Paolillo, M., et al. 2016, ApJL, 819, L31

Da Rocha, C., & Mendes de Oliveira, C. 2005, MNRAS, 364, 1069

Da Rocha, C., Ziegler, B. L., & Mendes de Oliveira, C. 2008, MNRAS, 388, 1433

De Lucia, G., Springel, V., White, S. D. M., Croton, D., & Kauffmann, G. 2006, MNRAS, 366, 499

DeMaio, T., Gonzalez, A. H., Zabludoff, A., et al. 2018, MNRAS, 474, 3009

Donzelli, C. J., Muriel, H., & Madrid, J. P. 2011, ApJS, 195, 15

Duc, P.-A., Cuillandre, J.-C., Karabal, E., et al. 2015, MNRAS, 446, 120

Feldmeier, J. J., Mihos, J. C., Morrison, H. L., Rodney, S. A., & Harding, P. 2002, ApJ, 575, 779

Ferrarese, L., Côté, P., Cuillandre, J.-C., et al. 2012, ApJS, 200, 4

Gerhard, O., Arnaboldi, M., Freeman, K. C., et al. 2005, ApJL, 621, L93

Gerhard, O., Arnaboldi, M., Freeman, K. C., et al. 2007, A&A, 468, 815

Ghosh, K. K., Swartz, D. A., Tennant, A. F., Wu, K., & Saripalli, L. 2005, ApJ, 623, 815

Gonzalez, A. H., Zabludoff, A. I., & Zaritsky, D. 2005, ApJ, 618, 195

Gourgoulhon, E., Chamaraux, P., & Fouque, P. 1992, A&A, 255, 69

Grado, A., Capaccioli, M., Limatola, L., & Getman, F. 2012, Memorie della Societa Astronomica Italiana Supplementi, 19, 362

Guhathakurta, P., Knapp, G. R., van Gorkom, J. H., & Kim, D.-W. 1990, NASA Conference Publication, 3084,

Hilker, M., & Kissler-Patig, M. 1996, A&A, 314, 357

Ibata, R. A., Lewis, G. F., McConnachie, A. W., et al. 2014, ApJ, 780, 128

Iodice, E., Capaccioli, M., Grado, A., et al. 2016, ApJ, 820, 42

Iodice, E., Spavone, M., Capaccioli, M., et al. 2017, ApJ, 839, 21

Iodice, E., Spavone, M., Cantiello, M., et al. 2017, ApJ, 851, 75

Kennicutt, R. C., Jr. 1998, ARA&A, 36, 189

Kim, D.-W., Jura, M., Guhathakurta, P., Knapp, G. R., & van Gorkom, J. H. 1988, ApJ, 330, 684

Krick, J. E., Bernstein, R. A., & Pimbblet, K. A. 2006, AJ, 131, 168

Krick, J. E., & Bernstein, R. A. 2007, AJ, 134, 466

La Barbera, F., Ferreras, I., de Carvalho, R. R., et al. 2012, MNRAS, 426, 2300

Leonardi, A. J., & Worthey, G. 2000, ApJ, 534, 650)

Lin, Y.-T., & Mohr, J. J. 2004, ApJ, 617, 879

Longobardi, A., Arnaboldi, M., Gerhard, O., et al. 2013, A&A, 558, A42

Longobardi, A., Arnaboldi, M., Gerhard, O., & Hanuschik, R. 2015, A&A, 579, A135

Malin, D. F., & Carter, D. 1983, ApJ, 274, 534

Martin, D. C., Fanson, J., Schiminovich, D., et al. 2005, ApJL, 619, L1

McGee, S. L., & Balogh, M. L. 2010, MNRAS, 403, L79

Merritt, A., van Dokkum, P., Danieli, S., et al. 2016, ApJ, 833, 168

Mihos, J. C., Harding, P., Feldmeier, J., & Morrison, H. 2005, ApJL, 631, L41

Mihos, C. 2015, IAU General Assembly, 22, 2247903

Morrissey, P., Schiminovich, D., Barlow, T. A., et al. 2005, ApJL, 619, L7

Morrissey, P., Conrow, T., Barlow, T. A., et al. 2007, ApJS, 173, 682

Muñoz, R. P., Eigenthaler, P., Puzia, T. H., et al. 2015, ApJL, 813, L15

Murante, G., Arnaboldi, M., Gerhard, O., et al. 2004, ApJL, 607, L83

Murante, G., Giovalli, M., Gerhard, O., et al. 2007, MNRAS, 377, 2

Napolitano, N. R., Pannella, M., Arnaboldi, M., et al. 2003, ApJ, 594, 172

Okamoto, S., Arimoto, N., Ferguson, A. M. N., et al. 2015, ApJL, 809, L1

Pillepich, A., Nelson, D., Hernquist, L., et al. 2018, MNRAS, 475, 648

Pohlen, M., & Trujillo, I. 2006, A&A, 454, 759

Purcell, C. W., Bullock, J. S., & Zentner, A. R. 2007, ApJ, 666, 20

Rampazzo, R., Marino, A., Tantalo, R., et al. 2007, MNRAS, 381, 245

Rampazzo, R., Panuzzo, P., Vega, O., et al. 2013, MNRAS, 432, 374

Ricciardelli, E., Vazdekis, A., Cenarro, A. J., & Falcón-Barroso, J. 2012, MNRAS, 424, 172

Rudick, C. S., Mihos, J. C., & McBride, C. 2006, ApJ, 648, 936

Seigar, M. S., Graham, A. W., & Jerjen, H. 2007, MNRAS, 378, 1575

Sérsic, J. L. 1963, Boletin de la Asociacion Argentina de Astronomia La Plata Argentina, 6, 41

Smith, B. J., Campbell, K., Struck, C., et al. 2018, AJ, 155, 81

Sommer-Larsen, J. 2006, MNRAS, 369, 958

Spavone, M., Capaccioli, M., Napolitano, N. R., et al. 2017, A&A, 603, A38

Tal, T., van Dokkum, P. G., Nelan, J., & Bezanson, R. 2009, AJ, 138, 1417

Tollet, É., Cattaneo, A., Mamon, G. A., Moutard, T., & van den Bosch, F. C. 2017, MNRAS, 471, 4170

Tully, R. B. 1988, Cambridge and New York, Cambridge University Press, 1988, 221 p.,

Vazdekis, A., Ricciardelli, E., Cenarro, A. J., et al. 2012, MNRAS, 424, 157

Watkins, A. E., Mihos, J. C., & Harding, P. 2015, ApJL, 800, L3

Watkins, A. E., Mihos, J. C., Harding, P., & Feldmeier, J. J. 2017, ApJ, 836, 145

Watson, D. F., Berlind, A. A., & Zentner, A. R. 2012, ApJ, 754, 90

White, P. M., Bothun, G., Guerrero, M. A., West, M. J., & Barkhouse, W. A. 2003, ApJ, 585, 739

Williams, B. F., Ciardullo, R., Durrell, P. R., et al. 2007, ApJ, 656, 756

Willman, B., Governato, F., Wadsley, J., & Quinn, T. 2004, MNRAS, 355, 159

Wright, E. L., Eisenhardt, P. R. M., Mainzer, A. K., et al. 2010, AJ, 140, 1868-1881

Zibetti, S., White, S. D. M., Schneider, D. P., & Brinkmann, J. 2005, MNRAS, 358, 949